

**THE DEVELOPMENT OF PROCESSING METHODS FOR A  
QUANTITATIVE HISTOLOGICAL INVESTIGATION OF RAT HEARTS**

A Thesis

by

EMILY HOPE JETTON

Submitted to the Office of Graduate Studies of  
Texas A&M University  
in partial fulfillment of the requirements for the degree of

MASTER OF SCIENCE

August 2004

Major Subject: Biomedical Engineering

**THE DEVELOPMENT OF PROCESSING METHODS FOR A  
QUANTITATIVE HISTOLOGICAL INVESTIGATION OF RAT HEARTS**

A Thesis

by

EMILY HOPE JETTON

Submitted to Texas A&M University  
in partial fulfillment of the requirements  
for the degree of

MASTER OF SCIENCE

Approved as to style and content by:

---

John Criscione  
(Chair of the Committee)

---

Jay Humphrey  
(Member)

---

Christopher Quick  
(Member)

---

William Hyman  
(Head of Department)

August 2004

Major Subject: Biomedical Engineering

## ABSTRACT

The Development of Processing Methods for a Quantitative Histological Investigation of Rat Hearts. (August 2004)

Emily Hope Jetton, B.S., Texas A&M University  
Chair of Advisory Committee: Dr. John Criscione

In order to understand the mechanical functions of the cardiac muscle it is important to first understand the microstructure of the tissue. Young et al. (1998) realized that quantitative three-dimensional information about the ventricular myocardium is necessary to analyze myocardial mechanics. They developed a technique using confocal fluorescence laser scanning microscopy to obtain three-dimensional images. While this method worked well in rebuilding the myocardial tissue image by image, it was quite extensive and costly. Costa et al. (1999) developed a method that was used to perform three-dimensional reconstruction as well. Their method, while less expensive and much less time consuming, required sheet assumptions and did not look directly at the cross-fiber plane.

From Dr. Criscione's previous work on canines (Ashikaga et al., 2004), we found that the sheet structure can be accurately determined from cross-fiber sections without making any sheet assumptions. We have now expanded on those ideas and created a method to perform the quantitative histological investigation of the rat hearts in a way that is both timely and cost effective. We developed a processing method that preserves the orientation of the fiber and sheet angles. This method was carried out using plastic embedding since the dehydration process used in paraffin embedding has a tendency to grossly distort tissue. Once the heart was fixed in formalin, we then removed the septum and sliced it several times vertically. This allowed us to image the tissue at several depths and find an average fiber angle for each slice. Next, the specimen was hardened, and the sheet orientation was evaluated using polarized light. Once both fiber and sheet angles were obtained from several depths within the septum, we then constructed a three-dimension model of the wall. This method was both cost effective and less time

consuming than previous ones and will be a method that can be used in the future to compare the myocardial tissue of diseased and healthy rat hearts so that we may better understand the mechanical functions of the heart as it remodels due to disease.

## **ACKNOWLEDGEMENTS**

I would like to thank Dr. John C. Criscione and Kristen K. Hudson for their help in the completion of this research which was funded by the American Heart Association grant number 0265133Y.

## TABLE OF CONTENTS

	Page
ABSTRACT .....	iii
ACKNOWLEDGEMENTS .....	v
TABLE OF CONTENTS .....	vi
LIST OF FIGURES .....	viii
LIST OF TABLES .....	ix
 CHAPTER	
I INTRODUCTION .....	1
1.1 Motivation and Rationale .....	1
1.2 Cardiac Dysfunction and Hypertrophy .....	3
1.3 Significance and Cardiovascular Relevance .....	5
1.4 Objectives .....	6
1.5 Goal of Thesis .....	7
II BACKGROUND .....	9
2.1 Structure of the Myocardium .....	9
2.2 Relevant Research on Quantitative Cardiac Microstructure .....	10
III MATERIALS AND METHODS .....	13
3.1 Overview of the Experimental Design .....	13
3.2 Heart Removal and Preservation .....	13
3.3 Slicing and Orientation Techniques .....	15
IV RESULTS .....	23
4.1 Introduction .....	23
4.2 Preliminary Measurements .....	23
4.3 Fiber Alignment through the Interventricular Septum .....	24
4.4 Sheet Alignment through the Interventricular Septum .....	26
4.5 Three-Dimensional Reconstruction .....	32

CHAPTER	Page
V DISCUSSION .....	34
5.1 Introduction.....	34
5.2 Discussion of Heart Removal and Preservation.....	34
5.3 Discussion of Slicing and Orientation Techniques.....	35
5.4 Fiber Alignment.....	35
5.5 Sheet Alignment.....	35
5.6 Three-Dimensional Reconstruction .....	36
5.7 Animal Model .....	36
VI CONCLUSIONS AND RECOMMENDATIONS .....	38
6.1 Conclusions.....	38
6.2 Recommendations.....	38
REFERENCES .....	40
VITA.....	43

## LIST OF FIGURES

	Page	
Figure 1.1	Normal heart, concentric hypertrophy due to volume overload, and eccentric hypertrophy due to pressure overload (Adapted from Braunwald, 2001).....	4
Figure 3.1	Slicing apparatus.....	16
Figure 3.2	Depiction of excised block of tissue from the interventricular septum	16
Figure 3.3	Cut tissue sample with faces (F) and slices (S) marked.....	17
Figure 3.4	Sample template for slice one.....	19
Figure 3.5	Slice one viewed perpendicular to the fiber direction.....	19
Figure 3.6	Sheet measurement program results.....	21
Figure 3.7	Example of two different sheet families seen in one slice.....	22
Figure 4.1	Sample of image used to take alpha measurements.....	24
Figure 4.2	Plot of fiber angle measurements from endocardium (face 1) to epicardium (face 2).....	25
Figure 4.3	Image of the cross-fiber view of slice one taken with digital camera from Biological Microscope.....	26
Figure 4.4	Plot of sheet angles taken from slice one.....	28
Figure 4.5	Plot of sheet angles taken from slice two.....	29
Figure 4.6	Plot of sheet angles taken from slice three.....	30
Figure 4.7	Plot of sheet angles taken from slice four.....	31
Figure 4.8	Three-dimension reconstruction using alpha and beta findings.....	33
Figure 5.1	Depictions of transverse tissue slices of the LV from Dahl salt-sensitive rats fed high salt diets at 6 wks, 11 wks, and 18 wks respectively (after Inoko, 1994).....	37



**LIST OF TABLES**

	Page
Table 4.1    Measurements of the left ventricle in diastole and septum thickness.....	23
Table 4.2    Average of fiber angle measurements and their standard deviations .....	25
Table 4.3    Average fiber angle in the center of each slice based on ten measurements.....	26
Table 4.4    Sheet angle results and $\beta$ estimate from slice one .....	28
Table 4.5    Sheet angle results and $\beta$ estimate from slice two .....	29
Table 4.6    Sheet angle results and $\beta$ estimate from slice three .....	30
Table 4.7    Sheet angle results and $\beta$ estimate from slice four.....	31

## CHAPTER I

### INTRODUCTION

#### *1.1 Motivation and Rationale*

The heart is a compact muscular pump which contracts nearly 2.5 billion times during the human life span. It is responsible for the compensation of acute changes in the demands for blood flow and adapts to sustain changes in applied loads (Humphrey, 2002). The heart consists of two pumps in series. Deoxygenated blood is drawn into the right atrium via the superior and inferior vena cava. The blood is then pumped out from the right ventricle through the pulmonary artery and sent to the lungs to become oxygenated. Oxygenated blood is brought into the left atrium through the pulmonary veins and then pumped from the left ventricle into the aorta which carries the oxygen rich blood to the systemic portions of the body. The atria are thin-walled, low pressure chambers which act more like large reservoir conduits for the blood than as significant pumps for its forward propulsion. The ventricles, however, are formed by a continuum of muscle fibers that start from the fibrous skeleton at the base of the heart and sweep up toward the apex at the epicardial surface. While passing toward the endocardium, they gradually undergo a 180-degree change in direction to lie parallel to the epicardial fibers and form the endocardium and papillary muscles. These fibers twist and turn inward at the apex to form the papillary muscles while at the base they form a thicker muscle that decreases the ventricular circumference during the ejection of blood. In addition to this reduction in circumference, ventricular ejection is also accomplished with a decrease in the longitudinal axis due to the descent of the base of the heart (Berne and Levy, 2001).

The wall of the heart is made up of three distinct layers, the inner, middle, and outer also known as the endocardium, myocardium, and epicardium respectively. The inside of each cardiac chamber is lined with endocardium which is about 100 $\mu$ m thick and consists primarily of a two-dimensional plexus of collagen and elastin as well as a single cell

---

This thesis follows the style of the Journal of Biomechanics.

layer of endothelial cells that serve as a direct interface between the blood and the heart wall. The myocardium, or parenchymal tissue, is the functional tissue of the heart which allows it to pump blood. The heart consists primarily of myocytes arranged into locally parallel muscle fibers which in turn are embedded in an extracellular matrix consisting largely of type I and III collagen. The orientation of these muscle fibers change with position in the wall of the heart. The epicardium is a thin serous layer also about 100  $\mu\text{m}$  thick consisting largely of two-dimensional plexus of collagen and some elastic fibers (Humphrey, 2002).

In the past, scientist such as LeGrice, Young, Costa, Arts et al. have studied the slippage of adjacent muscle layers along cleavage planes which have been shown to accommodate the substantial changes in the ventricular cavity dimension and wall thickness that occur during the cardiac cycle. This idea has also been used to explain aspects of the regional dilation of the ventricle and local wall thinning that occurs following myocardial infarction. Furthermore, remodeling of the cardiac extracellular connective tissue observed during chronic hypertension and aging has been linked to altered diastolic performance and impaired transverse electrical coupling (LeGrice et al., 1995a). Researchers also believe that the connective tissue matrix may be disrupted in acute myocardial ischemia and in stunned myocardium (LeGrice et al., 1995a). It has been discussed that this may contribute to the aberrant wall motion observed under hypertensive circumstances and the alteration of the mechanical properties of the affected regions.

Dr. Criscione stated in his proposed research with the American Heart Association that whereas most histological investigations of myocardium focus on its constituents (collagen and myocytes), myocardium functions as a composite structure with the fundamental unit being the myolamina. It is thought that this laminar structure evolved so as to permit large shear strains without developing large shear stresses that consume energy unnecessarily. Since there is a large transmural variation in shear strain, it is possible, and likely, that the myolaminar structure displays a transmural variation which likely changes with growth, remodeling, disease, and clinical intervention.

### *1.2 Cardiac Dysfunction and Hypertrophy*

Cardiac dysfunction can result from several mechanisms which often culminate during heart failure. These mechanisms include: failure of the pump itself when damaged muscle can not contract adequately and the chambers can not empty properly, regurgitant flow which occurs during mitral or aortic valvular regurgitation, disorders of cardiac conduction which occur during heart block or ventricular fibrillation, and obstruction to flow which occurs during aortic valvular stenosis, systemic hypertension, or aortic coarctation (Schoen, 1999). Congestive heart failure is a common and many times recurrent condition that currently has a rather poor prognosis and results in mortality for more than 50% in less than 5 years. It is the underlying or contributing cause of death in nearly 300,000 people in the US each year, and there are nearly 2 million individuals currently being treated. At this time, it is the leading diagnosis in discharged hospital patients over 65. Most instances of heart failure are a result of progressive deterioration of the myocardial contractile function. This is often caused by ischemic injury, pressure or volume overload, or dilation of cardiomyopathy (Schoen, 1999).

Heart failure is defined as a pathophysiologic state in which the cardiac function becomes abnormal causing the heart to fail to pump blood at a rate appropriate for the requirements of metabolizing tissue and/or allows it to do so only from an abnormally elevated diastolic volume (Braunwald, 2001). The ventricles respond to an increased hemodynamic load with the development of hypertrophy. This occurs when they are called on to deliver an elevated cardiac output for prolonged periods as in valvular regurgitation. At this point, the heart develops eccentric hypertrophy in which cavity dilation occurs, and the ratio between wall thickness and ventricular cavity size remains relatively constant in the early phases. With pressure overload, which occurs in valvular aortic stenosis or hypertension, concentric hypertrophy occurs and the ratio between the wall thickness and ventricular cavity size increases. This can be seen in figure 1.1. In both cases a stable hyper functioning state may go on for years, but the myocardial function may eventually deteriorate leading to heart failure. Often at this time the ventricle dilates and the ratio between wall thickness and diameter decreases leading to

increased stress on each unit of myocardium, further dilation, and a vicious cycle (Braunwald, 2001).

It is known that the heart grows and remodels in health (development and exercise hypertrophy) and disease (ventricular aneurysm, post MI, volume and pressure overload hypertrophy). Understanding how and why myocardium responds to its mechanical environment is the first step in developing rational treatments and /or tissue engineered replacements for the increasing number of Americans who suffer from heart disease.

This project focused on cardiac hypertrophy induced by hypertension. Since we will be inducing hypertension, in future rat models, the ventricles will be pressure overloaded which will lead to the development of pressure or concentric hypertrophy of the LV with an initial increase in wall thickness and normal to reduced ventricle diameter. This was seen in experiments conducted by Inoko et al. on Dahl salt sensitive rats. It was also seen that as failure progressed, the wall thickness decreased and the radius increased therefore decreasing the overall thickness to radius ratio (Inoko et al., 1994).

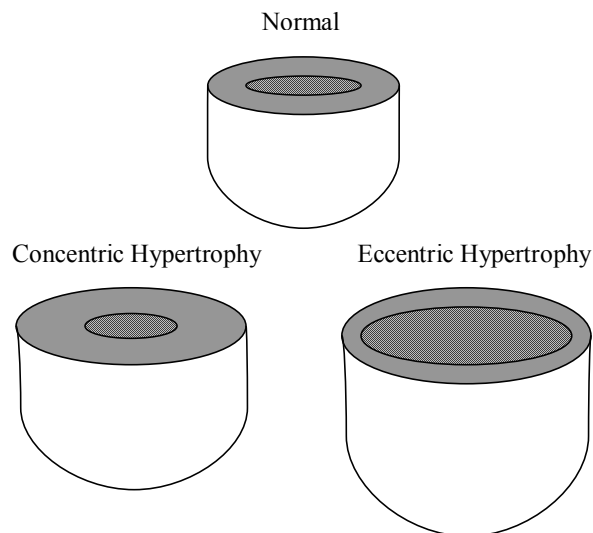


Fig. 1.1. Normal heart, concentric hypertrophy due to volume overload, and eccentric hypertrophy due to pressure overload (Adapted from Braunwald, 2001)

### 1.3 *Significance and Cardiovascular Relevance*

Through this research we sought to develop a method of analysis that can be used to better understand heart disease. While present treatments are continuously improving, there are still many things that we do not fully understand about the mechanics of cardiac growth and remodeling in both health and disease. Past researchers have found that altered hemodynamic loading and/or heart disease leads to growth and remodeling of myocytes and the extra cellular matrix (ECM) (Grossman, 1980). They have also found that myocytes and cardiac fibroblasts are highly mechano sensitive in the sense that even subtle mechanical stimuli can influence gene expression (Komuro and Yazaki, 1993, Sadoshima and Izumo, 1997). Therefore, it is possible, and quite likely, that mechanical stress or strain controls growth, orientation, differentiation, and contractile dysfunction of myocytes (Omens, 1998). Other possible controllers, or co-contributors in dilated cardiomyopathy, are loss of myocytes shortening capabilities (Figueredo and Camacho, 1994), calcium dysregulation (Feldman et al., 1993), and myocyte apoptosis (Sabbah and Sharov, 1998). With regard to mechanics, current ellipsoidal models of the heart with gross simplifying assumptions can give, at best, only an averaged stress value with little to no transmural variation. The problem with this simplification is that it is unlikely that such global types of stress results will be useful in investigating the growth and remodeling of myocardium due to anticipation that subtle differences in stress values will outweigh the cellular response.

In order to calculate the stress field so as to demonstrate the role of stress in cardiac growth and remodeling, it was necessary to use continuum mechanics and quantify the mechanical behavior of the myocardium (Costa et al., 2001). In the future, the analysis of healthy and diseased hearts will become important for defining both the material symmetry directions and transmural heterogeneities in the material properties. More importantly, many investigators now use myocyte cultures to investigate the cellular and molecular biology of myocytes and cardiac fibroblasts. However, a thorough knowledge of the microstructure will still be essential for integrating this information into models of the heart in both health and disease.

The functional significance of the seen laminar organization of myocytes and the gaps between the sheets appears to be that they allow myocardium to undergo large

shearing deformation without developing large counteracting shear stress (Caulfield and Borg, 1979, Costa et al., 1999). Due to the fact that the outer part of the LV wall undergoes much less shear deformation relative to the inner part of the wall (Costa et al., 1999), it stands to reason that transmural variation in laminar organization will exist if the laminar structure is directly modulated by shearing of the sheets. Our specific goal was to develop a method in which we could establish and quantify the transmural variations in the healthy as well as the diseased rat.

Through development, transmural variations in shearing deformation are present in the heart by virtue of it being a thick-walled pressure vessel. Therefore, a transmural variation in myolamina structure could be programmed into cardiac development or maintained by the continuous turnover of the ECM. To look into this further, we will need to quantify the myocardial microstructure of septae from Dahl salt sensitive volume overloaded rat hearts. As these hearts go into failure, they develop a much smaller thickness to radius ratio, whereby, transmural variations in shearing deformation are reduced (LeGrice et al., 1995a, Inoko et al., 1994). If transmural variation in myolamina structure shows similar reduction then we may conclude that laminar structure is modulated by ECM turnover. Conversely, the laminar structure of the aorta is static upon development such that the number of lamina in adults is held constant even during gross remodeling (Matsumoto and Hayashi, 1996). If the laminar structure of myocardium is similarly static, then the laminar structure of the volume-overloaded septum should be similar to that of normal septae.

#### *1.4 Objectives*

This project was originally designed to focus on three specific objectives concerning the laminar structure of the heart muscle. The first of these objectives focused on developing an accurate and effective slicing method to maintain orientation while obtaining the tissue and acquiring the appropriate measurements. This was the focus of this thesis. Now that the method has been developed, the following objectives can be met. They include quantifying the average or typical laminar microstructure of the interventricular septum of normal rats, and quantifying the average or typical laminar microstructure of the interventricular septum of volume over loaded Dahl salt sensitive

rats. It is known that the layered, or laminar structure of heart muscle, has a significant variation in tissue alignment from the inner to the outer wall of the heart. This variation is functionally important in understanding how the heart grows (increases wall mass) and remodels (redistributes its constituents). Understanding how and why the myocardium respond to their mechanical environment is the first step in the development of rational treatments or tissue-engineered replacement treatments for the increasing number of Americans who suffer from heart disease. To better understand how the myocardium responds, we need to characterize cardiac microstructure and bridge the knowledge gap between cellular/matrix processes and cardiac function. Where most histological investigations of myocardium focus on its constituents, the myocardium does function as a composite structure. The fundamental structural unit being the myolamina – a sheet of myocytes, which are about four cells thick, surrounded by a collagen weave. The myocardium is able to undergo large shearing deformation with out developing large shear stress. This is apparently due to the functional significance of the laminar organization of myocytes and the gaps between the sheets. Since the outer part of the LV wall undergoes much less shear deformation relative to the inner part of the wall, it stands to reason that a transmural variation in laminar organization will exist if the laminar structure is directly modulated by shear. The larger number of cleavage planes, between the myolamina, allow for a larger development of shear from the inner to outer wall. Since the large transmural variation in shear strain is evident, it is possible, and likely, that the myolaminar structure displays a transmural variation which is likely to change with growth, remodeling, and disease. This hypothesis will be investigate in the near future. The existence or lack of such a transmural variation is important for integrating the knowledge of cells and ECM into a physiological understanding of how the heart functions via computer modeling.

### *1.5 Goal of Thesis*

The goal of this project was to develop an accurate and efficient slicing method to obtain samples to be used in quantifying the microstructure of rat myocardium. Based on Dr. Crisciones's past work on canine myocardium (Ashikaga et al., 2004), we hypothesized that the laminar microstructure of rat myocardium could be accurately and



quickly quantified by using slicing methods that allowed sections to be made perpendicular to the myofiber. The slices were then marked to maintain appropriate orientation and imaged so that they could later be reconstructed in an organized fashion. This allowed us to quantify the myocardial microstructure in this as well as future experiments on rat hearts so as to determine how and why the heart grows and remodels in conditions such as congestive heart failure.

## CHAPTER II

### BACKGROUND

#### *2.1 Structure of the Myocardium*

The anatomy and structure of an organ as vital as the heart has been the focus of many investigations. While it is commonly accepted that cardiac tissue consists of discrete layers of muscle with the ventricles being made of nested muscle bundles characterized by a well-defined helical fiber path running from the apex to base, quantitative studies of muscle fiber orientation within the ventricular wall have failed to confirm this distinct organization (LeGrice et al., 1995a). Many investigations have been and remain qualitative or pictorial treatments of the cardiac structure and myofiber orientation. However, the first quantitative investigations began in 1969 by Streeter (Streeter, 1979). Rather than the past beliefs that myocardium consisted of bundles of muscle fibers, the current view of myocardium is that of a continuum composed of myofibers that vary smoothly in direction as they go from the LV chamber to the outer LV surface (LeGrice et al., 1995). The laminar structured myocardium contains sheets of strongly coupled fibers separated by cleavage planes. These sheets, which are about four cells thick and directed radially across the ventricle, continually branch and interconnect both across and around the wall to form a strongly integrated three-dimensional structure with three axes of material symmetry at each point in the myocardium (LeGrice et al., 1997). Although this laminar structure (or fundamental structural unit) is well established, few have actually studied its morphology. Indeed, the current focus by most continues to be on its constituent parts, isolated myocytes (Gerdes and Capasso, 1995, Deschepper et al., 2002) and ECM (Robinson et al., 1983, Robinson et al. 1988). This project proposed to develop a method to fill this knowledge gap and quantify how the collagen sheets and myolamina intertwine to form the microstructure of this composite tissue that is myocardium in both healthy and in diseased hearts.

Due to past research done by LeGrice, Young, Nielsen, Arts et al., we have a much better understanding of the fiber and sheet angles in the heart and how they align from the

inner to outer wall. Their thorough dissection and imaging methods have descriptively laid out the true structure of myocardium. They have allowed us to focus more on the morphology of the collagen sheets and myolamina and how they intertwine to form the microstructure of this composite tissue that is myocardium in both healthy and diseased hearts. Therefore, we developed a more simplified method of three-dimensional reconstructions from two-dimensional images with fewer imaged slices. The method they used to fully characterize the microstructure of the rat heart was similar to our goal, except that we developed a more efficient method (Young et al., 1998) so that in the future we can compare the microstructure in multiple hearts of a disease model while matching controls.

## *2.2 Relevant Research on Quantitative Cardiac Microstructure*

Ventricular myocardium consists of a complex three-dimensional structure that has been inferred previously from two-dimensional images. Researchers have been working on quantifying the microstructure of the hearts for years (Nielsen et al., 1991, LeGrice et al., 1997, Young et al., 1998, Streeter, 1979). Streeter and Bassett were two of the first to begin quantifying measurements of fiber orientation through the heart wall. They found smooth transmural variation of fiber orientation and started the argument that the myocardium was a continuum rather than an assembly of discrete fiber bundles (Streeter and Bassett, 1966). Since that time, there have been quite a few studies of myocardial fiber orientation performed. While these studies mapped the muscle fiber orientation at a limited number of transmural ventricular sites, the fiber architecture was not quantitatively referred to ventricular geometry. Therefore, the data obtained provided a more qualitative than quantitative description of the cardiac fiber distribution within the myocardium (Nielsen et al., 1991).

Nielsen et al. (1991) performed extensive measurements on the transmural and regional variation of myofiber angles and composed a finite element model of the geometry and fibrous structure of the canine heart. He developed a mathematical representation of ventricular geometry and muscle fiber organization using three-dimensional finite elements referring to a prolate spheroid coordinate system. This research confirmed that the myocardial fibers follow the expected left-hand helical

pathway as viewed from the base of the epicardium, where as the endocardium, fiber orientation is reversed (Nielsen et al., 1991). This was a great first step in implementing a realistic mathematical description of the three-dimensional geometry of the ventricles as well as accurately representing the muscle fiber orientation. Later, LeGrice et al. (1997) extended the previous model of cardiac anatomy described in Nielsen 1991 to provide a more complete description of the cardiac microstructure by focusing more on the laminar structure of the canine heart (LeGrice et al., 1997). They defined three axes at each point in the myocardium: one in the fiber direction, one in the myocardial sheet plane at a right angle to the fibers, and the third normal to the sheet plane. This way of defining the orientation of the microstructural axes relative to the ventricular wall, rather than to some external reference, helped in the comparison between hearts of different size and shape (LeGrice et al., 1997) and was used in our research when finding  $\alpha$  (the fiber angle) and  $\beta$  (the sheet angle) in a variety of hearts.

Over the years, the functional importance of the laminar organization of the myocardium has been discussed at length (LeGrice et al., 1995a). Experimental studies on myocardial deformation have provided evidence to support the idea that cleavage planes in myocardium support the rearrangement of muscle fiber bundles during wall thickness changes with this rearrangement arising through shearing deformation between the myocardial laminae (LeGrice et al., 1995b). In previous work, it has been shown that for the subendocardial regions (where wall thickening is greatest) the direction of shearing deformation is consistent with a model of wall thickening based on the sheets sliding along myocardial cleavage planes (LeGrice et al., 1995b, LeGrice et al., 1997). From the comparison of laminar architecture and maximum strain vectors, it has been demonstrated that for the inner third of the wall, maximum shearing deformation is a resultant of relative sliding between myocardial laminae (LeGrice et al., 1997).

Young et al. (1998) later developed a method in rats to fully characterize the microstructure of the heart. This method is similar to how we carried out our goal, except that we proposed to develop a slicing method that is more efficient. In Young et al. (1998)'s method, entire tissue blocks were imaged one "slice mosaic" at a time. In order to do this, the tissue block was imaged at multiple depths with confocal microscopy at  $1.56 \mu\text{m}^2$  per pixel. The block was then removed, shaved down  $40 \mu\text{m}$ , replaced and

imaged at new depths. When reconstructed and viewed at any angle or slice using OpenGL, it is quite impressive, but, it is not a practical method for comparing the microstructure of multiple hearts.

We have now developed a method in which the septum of the heart can be quantified with orientation maintained in the same manner only more efficiently. By developing this new method we have made it possible to quantify multiple hearts at different stages of heart failure which, in the future, will allow us to better understand the development from a quantitative perspective. Dr. Criscione believes that transmural variation in sheet morphology should be less as wall thickness to radius ratio decreases, and therefore needed a method in which it will be possible to evaluate multiple hearts in a timely fashion.

## CHAPTER III

### MATERIALS AND METHODS

#### *3.1 Overview of the Experimental Design*

This chapter discusses the methods used to accomplish the goal of this research. Prior to detailing the methods involved, it is first important to understand why the interventricular septum was used as an ideal model for the investigation of myocardial microstructure. The excised septum is nearly planar with uniform thickness such that a simple coordinate system can be used to reconstruct the three-dimensional microstructure from histological sections. It is also important to note that there are no papillaries or trabeculae on the LV side of the septum and few trabeculae and small papillaries on the RV side. Therefore, the inner LV and outer RV surfaces of the LV septal wall are fairly well delineated by smooth endocardial membranes and there are no trabeculae-corne interfaces (Streeter, 1979) to cause fiber dispersion. As a result, the myofibers in the septum are nearly parallel to the plane of the wall. Therefore, tissue sections parallel to the wall are parallel to the myofiber as well. In contrast to the septal wall, the LV free-wall has much curvature, large papillaries, dramatic changes in wall thickness, and much more fiber dispersion. Since this research investigated the transmural variations in myolaminar morphology and remodeling, the unnecessary complexities of the LV free-wall were appropriately avoided.

Though there are many cardiac pathology studies that use swine and canine hearts, we decided to use rats due to the current trend in cardiac research toward the use of rodents. Also, to our advantage, genetically modified rodents are readily available and tremendously useful for investigating the genetic and sub-cellular mechanisms involved in growth, remodeling, and heart disease.

#### *3.2 Heart Removal and Preservation*

In the future, in order to best quantify this experiment, twenty Dahl salt sensitive rats will be purchased. Ten will be fed normal diets, and ten will be fed high salt diets

upon their arrival. They will be purchased at 15 weeks old. Upon arrival, four will be sacrificed at the age of 15 weeks; two from the normal group and two from the high salt group. We will then sacrifice two more normal and two more high salt rats at 16 and 17 weeks. The remainder will be sacrificed past 17 weeks based on the high salt rat's individual health. For each high salt sacrifice there will be a normal sacrifice.

In order to test our current method, a Sprague Dawley rat was anesthetized using a CO<sub>2</sub> chamber. The heart was exposed via a midline sternotomy. An 8-10mL bolus of ten mmol potassium chloride in phosphate buffered saline was injected rapidly into the LV via a 21 gage needle inserted through the apex of the heart, therefore, causing immediate cardiac arrest. The heart was then excised, weighed, and placed in the saline solution.

Next, the left and right atria were removed so that a small balloon could be placed in the LV cavity. This balloon was fastened to tubing which was tied tightly to the aorta to secure the heart. The tubing was then attached to a syringe filled with water at a set height of 10 cm above the formalin level in a 20mL beaker. This kept the heart pressurized at 1kPa. While 10 cm of water is a little higher than the normal central venous pressure of 5 to 7 cm of water, by increasing the pressure a little we were ensured that the heart was fixed in a definite state of diastole. Following this, the heart was placed in formalin and allowed to fix for 15 minutes. After 15 minutes, the balloon was removed and the heart was placed back in the formalin for a week to complete the fixation process.

After a week, the heart was removed from the formalin. The right ventricle was removed, and the diameter of the heart was measured from the posterior to anterior side and the left to right side. The interventricular septum was then removed and cut down to 5mm in the circumferential direction and 11mm in the longitudinal direction to fit into the slicing apparatus. Following this, the thickness was measured and recorded. The septum was then imaged on the LV side via light microscopy so that the fiber angle,  $\alpha$ , could be measured and recorded ( $\alpha$  is the angle that the myofiber makes counterclockwise from the circumferential direction). The septum was not measured on the RV side since the fiber angles were not clear due to some general fiber disarray. The RV  $\alpha$  angle was found using a linear equation we deduced from the other face

measurements (discussed further in results section). Prior to each cut, the tissue was marked with suture at the apex/posterior region so that orientation could be established throughout the imaging and cutting process. The septum was then sliced (refer to slicing techniques) at half its thickness and the midsection was imaged. Following this, the sample was then sliced at  $\frac{1}{4}$  and  $\frac{3}{4}$  its initial thickness and imaged again. The four slices were then infiltrated with JB-4 embedding solution for one week until the tissue appeared translucent and sank to the bottom of the centrifuge tube. The solution was changed after a day to ensure optimal infiltration.

Once the slices were properly infiltrated, they were removed and cut cross-fiber using templates designed based on each slice's individual  $\alpha$  measurements (refer to slicing section). Once cut, the slices were placed in a mold filled with JB-4 hardener and placed in a somewhat airtight container (we used a sealable plastic bag) for one to two days in the freezer until hardened appropriately. Following which, they were sliced using a microtome, and their  $\beta$  angles were measured ( $\beta$  is the angle that the laminar sheets make counterclockwise from the radial direction).

### 3.3 *Slicing and Orientation Techniques*

Our goal was to obtain fiber angles at several different depths from endocardium to epicardium in a quick and efficient manner while maintaining proper orientation. In order to do this, we had to develop our own slicing apparatus which could slice the samples smoothly and evenly. We knew the sample would have to be held firmly and cut quickly in order to avoid tearing or disfiguration during the slicing. Therefore, we designed a slicing apparatus in which the tissue sample could be placed and held in a rigid fashion and then a blade could be brought down through the center of the tissue in a quick fluent manner (fig. 3.1)

Since we knew that the fiber angles change gradually from the inner to the outer wall based on previous studies (LeGrice et al., 1995a, Young et al., 1998, Nielsen et al., 1991), we were able to collect sufficient data by just looking at four faces and taking the average to obtain fiber angles as they changed from inner to outer wall. The fiber angle was measured counterclockwise with respect to the positive circumferential direction as seen in figure 3.2.



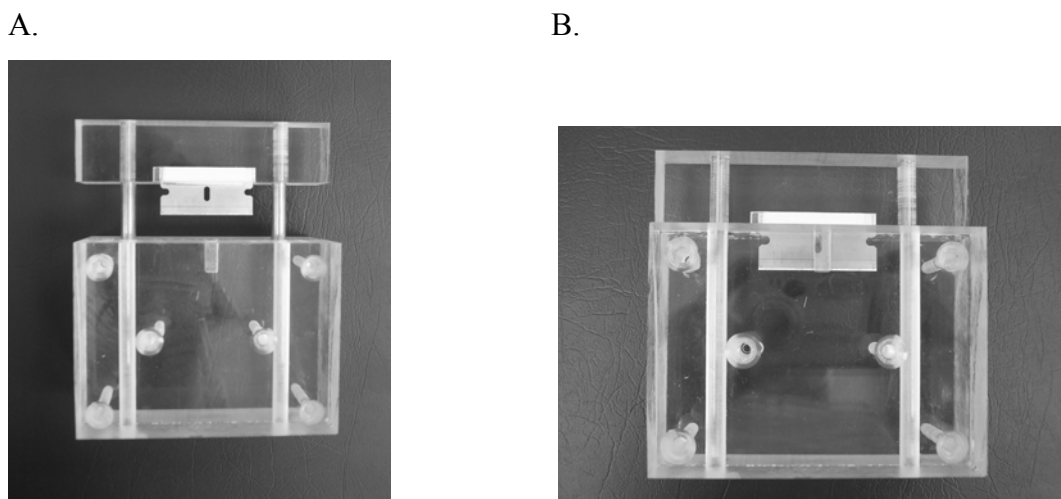


Figure 3.1 Slicing apparatus. A) Before cut. B) After cut.

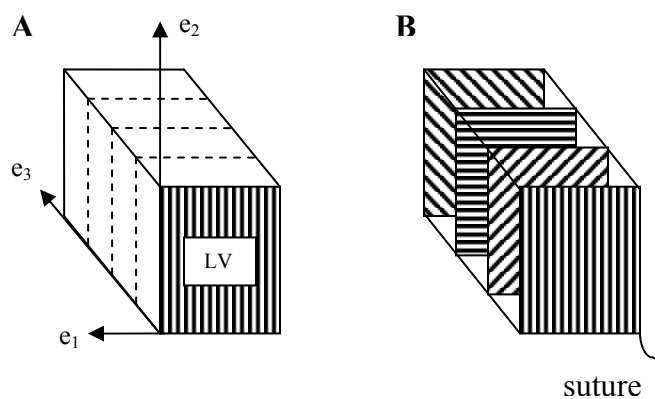


Fig. 3.2 Depiction of excised block of tissue from the interventricular septum. A) Viewed from inner LV wall. Markers used to define cardiac coordinated ( $e_1$ ,  $e_2$ ,  $e_3$ ) aligned with the local circumferential ( $e_1$ ), longitudinal ( $e_2$ ), and radial ( $e_3$ ) axes of the septum. B. Bold lines indicate hypothetical fiber angles measured counterclockwise from the positive circumferential direction. Suture depicts apex/posterior side.

First the  $\alpha$  angle was measured on the LV face of the sample or face one in 3, 5, 10 and 15 locations. This was done quickly using a computer generated angle measurement program called ImageJ (NIH). By measuring a number of angles, we were then able to take an average and get a more accurate idea of the actual  $\alpha$  measurement on the face, and by looking at the standard deviation from each group, we were able to come up with a sufficient number of angles to measure in the future. Paper was then attached to faces one and five along with a suture marking the apex toward the posterior side of the septum. This allowed us to maintain orientation while taking two-dimensional images from the slices. The tissue was then placed in the slicing device and cut. Once cut, face three was revealed. The  $\alpha$  measurements were taken off face three and recorded. Measurements could have been taken from either slice three or two depending on which looked better as long as we documented which slice the image came from.

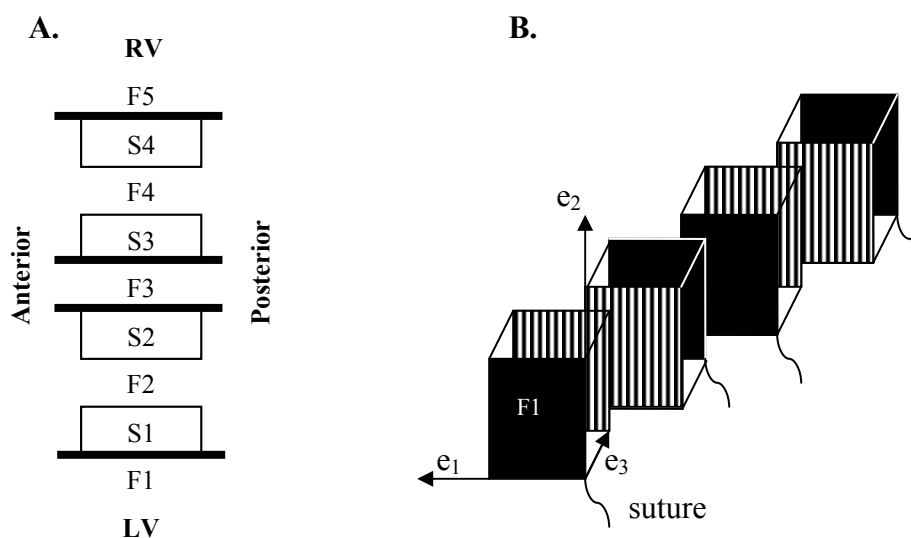


Fig. 3.3 Cut tissue sample with faces (F) and slices (S) marked. A) View from base directly down on tissue. Solid dark lines indicate faces with paper marking attached. B) View from face one, or the LV face, looking toward the outer RV side. Solid faces indicate those with paper marking and suture which is on the posterior/apex side. Vertical lines indicate faces with no paper marking. ( $e_1$ ,  $e_2$ ,  $e_3$ ) local circumferential, longitudinal, and radial axes of the septum respectively.

The Paper and string were then attached to both surfaces of face three and each slice was halved again revealing faces two and four.  $\alpha$  was measured and recorded from these faces as well (fig. 3.3).

Once a collection of measurements were obtained from each face, they were averaged to find the mean  $\alpha$  for each of the four faces. The next cut was made perpendicular to the fiber direction found in the center of each slice. The center  $\alpha$  value was found by taking the mean  $\alpha$  measurement of face one and face two which gave us the fiber angle in the center of slice one. This was repeated for each of the four slices to obtain the center fiber angle. In order to find the center of slice four, since face five was not measure due to fiber disarray, we fit a linear equation to the collected data and found the estimated face five  $\alpha$  from the equation and then took the mean of face four and five. The unit vectors for the fiber and cross-fiber were determined using the following equations:

$$\text{fiber} = \cos \alpha e_1 + \sin \alpha e_2, \quad (1)$$

$$\text{cross-fiber} = -\sin \alpha e_1 + \cos \alpha e_2. \quad (2)$$

Once the cross fiber was found, it was marked on the cutting template along with the fiber vector,  $e_1$ ,  $e_2$ , and  $e_3$  (the method used to reproduce the angles on the template is significant to one degree) (fig. 3.4). The slice was then glued to the template, paper side down, and cut along the cross-fiber marking in the upper 1/3 of the slice. The excess paper was then folded away from the positive cross-fiber and toward the negative cross-fiber to maintain orientation while imaging and placed in a mold cut side down. The mold was then filled with the JB-4 hardening solution and left for at least two days or until hardened. It was placed in the freezer to minimize air bubbles around the tissue while setting.

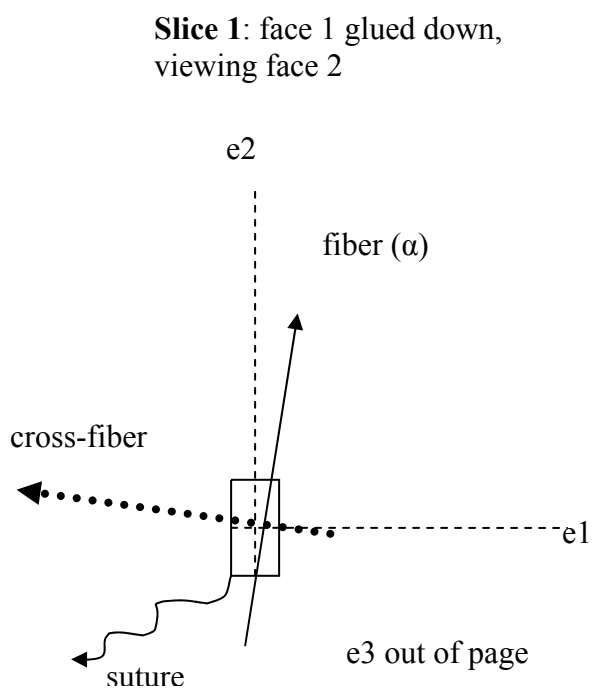


Fig. 3.4 Sample template for slice one. The suture is on the apex/posterior side to mark orientation. The dotted line marks where the slice was cut to obtain a cross-fiber view.

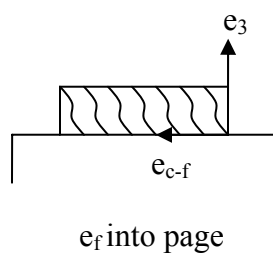


Fig. 3.5 Slice one viewed perpendicular to the fiber direction. Markers were used to define the cardiac coordinates ( $e_{c-f}$ ,  $e_f$ ,  $e_3$ ) aligned with the cross fiber ( $e_{c-f}$ ), fiber ( $e_f$ ), and radial ( $e_3$ ) axes of the septum. The curved lines indicate hypothetical sheet angles which were measured counterclockwise from the positive radial direction.

Once the sample hardened, it was removed from the mold and sliced using a microtome. The slices were then placed on glass slides and imaged using polarized light. The sheet angle  $\beta$  was measured from the positive radial direction at several locations and analyzed to give an appropriate  $\beta$  measurement for that particular slice. The slices looked similar to that seen in figure 3.5. In order to obtain the angle, we first had to collect data points from around the edge of each sheet in the image. These points were then put into a program that filled in the remainder of points to make a complete set of pixels to represent the sheet. The centroid, or average pixel position, was then located by summing all the pixel's coordinates and dividing by the total number of pixels  $N$ . Once the centroid was found we then used the equation

$$\sum_{i=1}^N \frac{r^{(i)} \otimes r^{(i)}}{N} = \frac{1}{N} \begin{bmatrix} \sum_{i=1}^N r_x^{(i)} r_x^{(i)} & \sum_{i=1}^N r_x^{(i)} r_y^{(i)} \\ \sum_{i=1}^N r_y^{(i)} r_x^{(i)} & \sum_{i=1}^N r_y^{(i)} r_y^{(i)} \end{bmatrix} \quad (3)$$

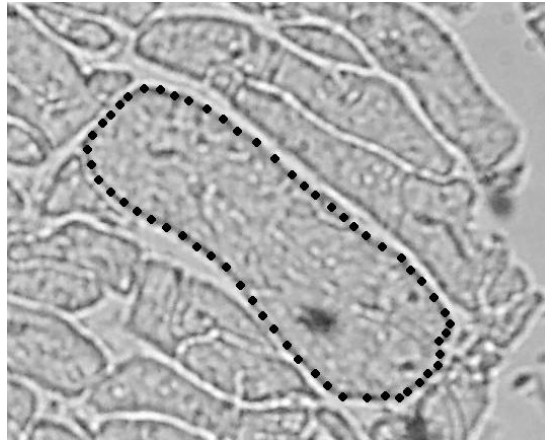
to find the symmetric tensor which provided us with a principal value and direction. In this equation  $r$  is the vector that goes from the centroid to each pixel  $i$ . The greatest principal value and direction are both associated with the major axis with the principal value being the square of the major axis of the ellipse if the sheet cross-section was perfectly elliptical. Since most of the sheets were not perfectly elliptical, this program actually found the effective major axis (fig. 3.6). This was sufficient since we were only concerned with finding the angles. The program returned the  $x$  and  $y$  coordinates of the major axis' unit vector. We then used

$$\text{Sheet angle} = -\tan^{-1} \frac{y}{x} \quad (4)$$

to find the sheet angle. In order to find an appropriate  $\beta$  it was important to evaluate the sheets carefully, and notice that some belonged to different sheet families such as those seen in figure 3.7. Because of this, we could not just average all the sheets within our region of interest. We instead grouped the sheet angles into several bins, based on the

number of angles collected and found the average of the largest bin. This allowed us to obtain the  $\beta$  measurement of the predominate sheet family.

A.



B.

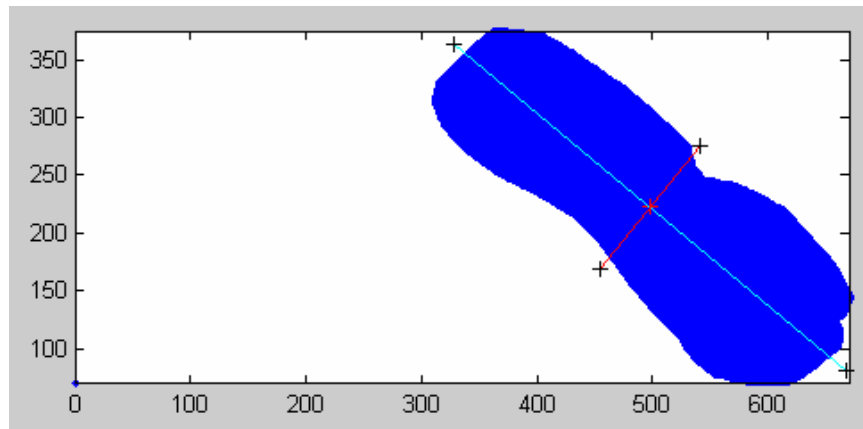


Fig. 3.6 Sheet measurement program results. A) Shows the data points collected off the image using the program ImageJ. B) Shows how our program recreates the image by filling in the remaining data points and finding the minor and major axis.

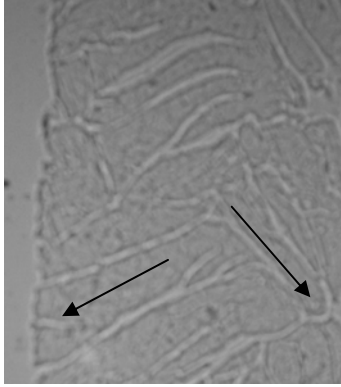


Fig. 3.7 Example of two different sheet families seen in one slice.

## CHAPTER IV

### RESULTS

#### 4.1 Introduction

In this section, the measured fiber and sheet angles are reported as well as the three-dimensional reconstruction of the two-dimensional images using the obtained angle measurements.

The rats used for our initial test were Sprague Dawley. They were sacrificed using a CO<sub>2</sub> chamber and the hearts were immediately extracted and fixed as discussed in the methods section. We used the Olympus SZX12 (Olympus Optical Co Ltd., Tokyo, Japan) to obtain the fiber angles, and the Olympus CX31 Biological Microscope (Olympus America Inc., Melville, NY) with the Kodak Easy Share DX4900 Zoom Digital Camera (Eastman Kodak Company, Rochester, NY) to obtain the sheet results.

#### 4.2 Preliminary Measurements

Once the heart was fixed, it was important to measure it prior to removing the septum in order to know the size of the LV during diastole. This will become more crucial when comparing healthy and diseased rats. The extracted heart was measured from anterior to posterior and from left to right. Once these measurements were made, the septum was removed and the thickness was measured. The results are seen in Table 4.1.

Table 4.1 Measurements of the left ventricle in diastole and septum thickness.

Posterior to anterior measure:	10.8 mm
Left to right measure:	10.9 mm
Thickness:	2.9 mm



### 4.3 *Fiber Alignment through the Interventricular Septum*

This section quantitatively describes the fiber angles found in the septum from endocardium to epicardium. After the LV face was imaged, the sample was cut in half and face three was imaged and recorded. The sample was cut at  $\frac{1}{4}$  and  $\frac{3}{4}$  its depth and imaged each time using the Olympus SZX12. This allowed us to obtain clear images which could be used to collect our desired measurements using ImageJ (Fig. 4.1).

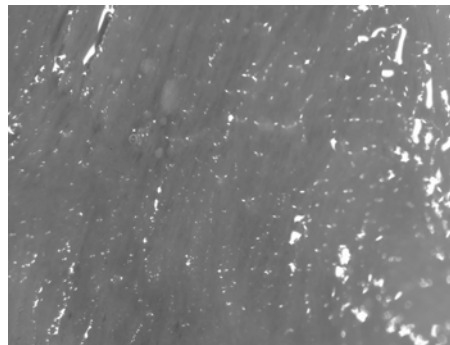


Fig. 4.1 Sample of image used to take alpha measurements.

Once the images were obtained, the angles were measured in several locations on the face of each slice. The measurements were then averaged, compared, and plotted. Table 4.2 shows the results of the measurements.

We took several groups of averages to verify our methods and make sure that we were able to obtain repeatable results. As can be seen, the standard deviation began to level out between 10 and 15 measurements. Therefore, we chose 10 measurements as sufficient to obtain valid fiber angles on each face. Figure 4.2 verifies our assumption that the fiber angles change smoothly in a uniform fashion from endocardium to epicardium. We plotted the average of several groups of measured data points to show that we had a good representation of  $\alpha$  at each face. Since we decided ten was sufficient, we used those measurements to find the line of best fit for the linear equation. By finding a linear equation based on the four slices, we are able to estimate the fiber angles at various depths through the septum with fewer slices and images. Once this was verified,

we then found the fiber angle in the center of each slice by averaging the fiber angle on the faces of either side of the slice. Using the measurements found, which are noted in table 4.3, we were then able to cut the slices cross-fiber using the designed templates mentioned in the methods section of this report. Once each slice was cut, we analyzed the cross fiber face and evaluate the sheet alignments which will be discussed in the following section. The significant digits were determined by the researcher's ability to align the samples prior to collecting the images. We felt that this was the greatest source of error in our measurements, however a one degree significant digit will be fine for the purpose of this research.

Table 4.2 Average of fiber angle measurements and their standard deviations.

		<b>Face 1</b>	<b>Face 2</b>	<b>Face 3</b>	<b>Face 4</b>	<b>Face 5 (eq)</b>
Averages	3	81	68	19	4	
	5	77	66	26	3	
	10	79	66	24	-2	-29
	15	78	65	25	-3	
Std. Devs.	3	6	6	1	9	
	5	7	5	3	8	
	10	5	5	6	12	
	15	5	6	5	11	

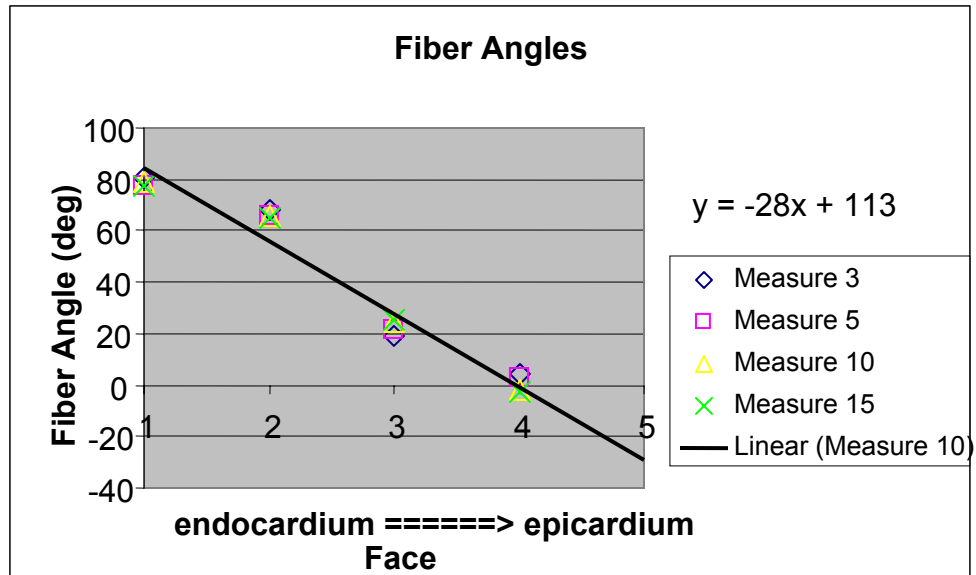


Figure 4.2 Plot of fiber angle measurements from endocardium (face 1) to epicardium (face 2).

Table 4.3 Average fiber angle in the center of each slice based on ten measurements.

<b>Slice 1</b>	72
<b>Slice 2</b>	45
<b>Slice 3</b>	11
<b>Slice 4</b>	-15

#### 4.4 Sheet Alignment through the Interventricular Septum

After each slice was cut cross-fiber, labeled, and hardened, it was then cut using a microtome and imaged on the Olympus CX31 Biological Microscope. This allowed us to obtain clear images which could be used to collect our desired  $\beta$  measurements (Fig. 4.3).

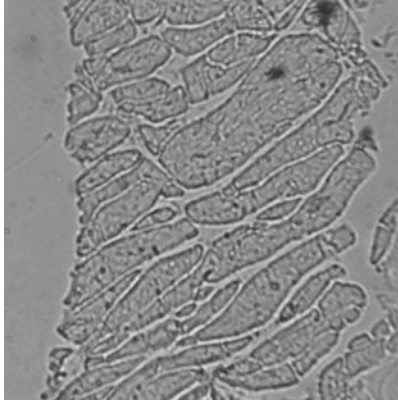


Fig 4.3 Image of the cross-fiber view of slice one taken with digital camera from Biological Microscope

In order to quantify the sheets within the septum, we did several analyses. First, we determined the orientation of the image based on where the paper was located. The positive cross-fiber direction was marked with the paper folded away from the sample. We could also determine the positive radial direction based on the slice we looked at, and the side of the slice the paper was on. We oriented all the images with the radial direction pointing left and the cross-fiber direction pointing upward. After this, we were able to zoom in and capture the images needed to obtain  $\beta$  measurements. Next, we determined which sheets we could use to collect the most accurate measurements. It was important that if the sheet was incomplete, that its major axis was the one that was cut off and not the minor in order to avoid inaccurate results. It was also important to make sure the sheets had not been disturbed during the fixation or slicing process. After this, we collected data points around each sheet using ImageJ and saved them as data files. We then used the data to find the major axis vector which was used to determine the angle each sheet made with respect to the positive radial direction. This allowed us to further analyze the sheets alignment through the septum wall. These results can be seen in tables 4.4-7 and figures 4.4-7. The significant figures for the sheet angles were also determined by the researcher's ability to align the samples prior to collecting the images.

Table 4.4 Sheet angle results and  $\beta$  estimate from slice one.

$-60 \leq x < -50$	$-50 \leq x < -40$	$-40 \leq x < -30$	$-30 \leq x < -20$	$-20 \leq x < -10$	$-10 \leq x < 0$	$0 \leq x < 10$
	-43	-40	-29	-16	-9	
	-41	-40	-29	-15		
		-40	-25	-11		
		-38	-23			
		-34	-22			
		-33	-21			
		-33	-21			
		-31	-21			
			-21			
					$\beta$ estimate =	-24

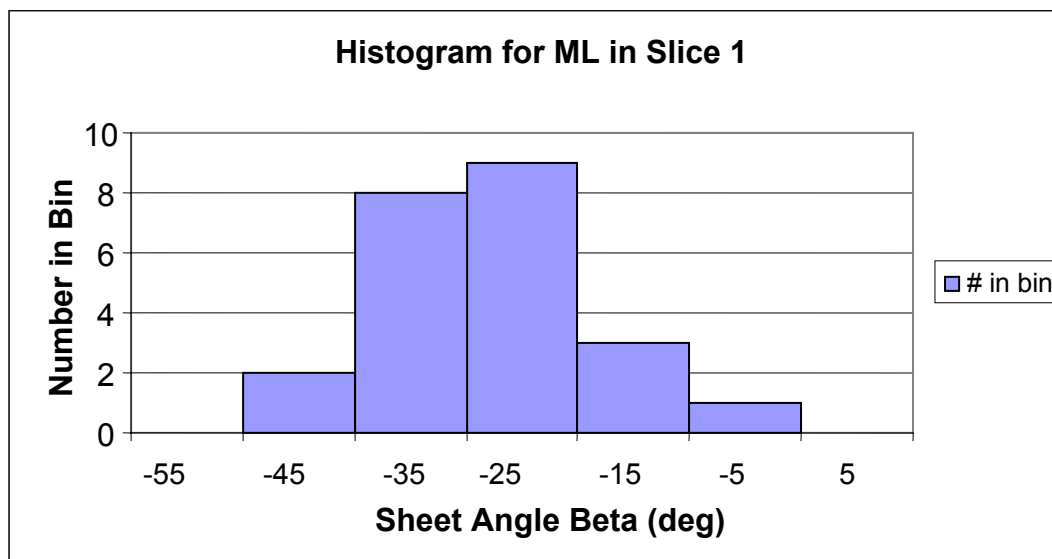


Fig. 4.4 Plot of sheet angles taken from slice one.

Table 4.5 Sheet angle results and  $\beta$  estimate from slice two.

$20 \leq x < 25$	$25 \leq x < 30$	$30 \leq x < 35$	$35 \leq x < 40$	$40 \leq x < 45$	$45 \leq x < 50$
	27	31	35	40	
	29	31	36	41	
	29	34	36	41	
	29	34	36	41	
			36		
			37	<b><math>\beta</math> estimate =</b>	<b>36</b>
			37		

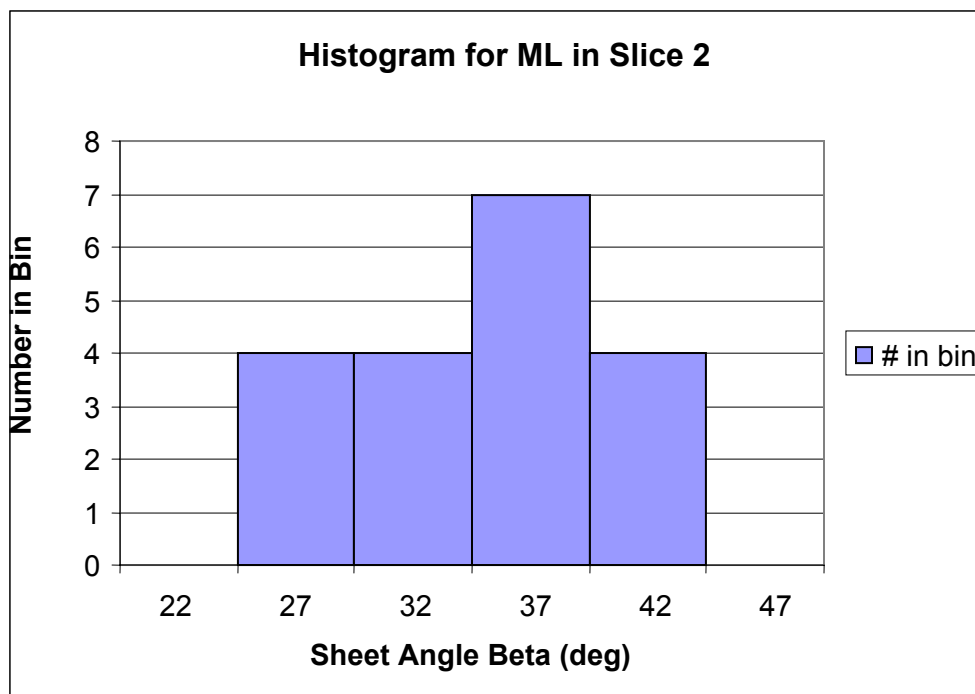


Fig. 4.5 Plot of sheet angles taken from slice two.

Table 4.6 Sheet angle results and  $\beta$  estimate from slice three.

$10 \leq x < 20$	$20 \leq x < 30$	$30 \leq x < 40$	$40 \leq x < 50$	$50 \leq x < 60$
	21	32	41	
	23	32	45	
	25	33	48	
	27	36		
		36		
		38		
		38	<b><math>\beta</math> estimate =</b>	<b>36</b>
		39		

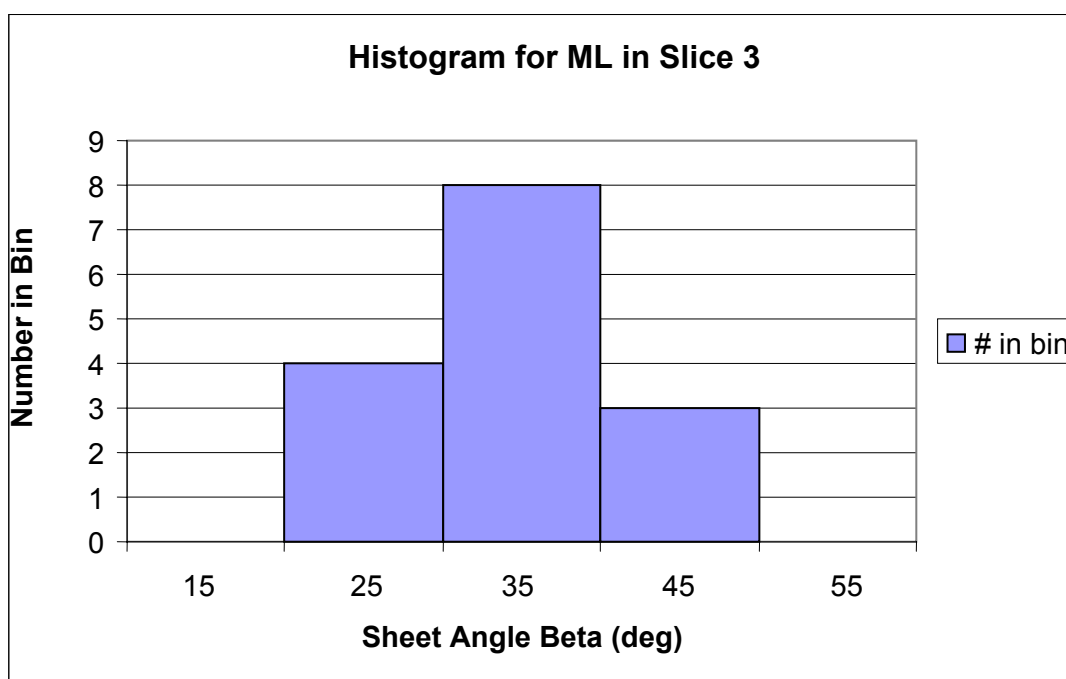


Fig. 4.6 Plot of sheet angles taken from slice three.

Table 4.7 Sheet angle results and  $\beta$  estimate from slice four.

$-63 \leq x < -55$	$-55 \leq x < -47$	$-47 \leq x < -39$	$-39 \leq x < -31$	$-31 \leq x < -23$	$-23 \leq x < -15$
	-54		-38	-31	
			-36	-29	
			-35	-29	
			-35		
			-34		
			-34		
			-32	<b><math>\beta</math> estimate =</b>	<b>-34</b>
			-32		

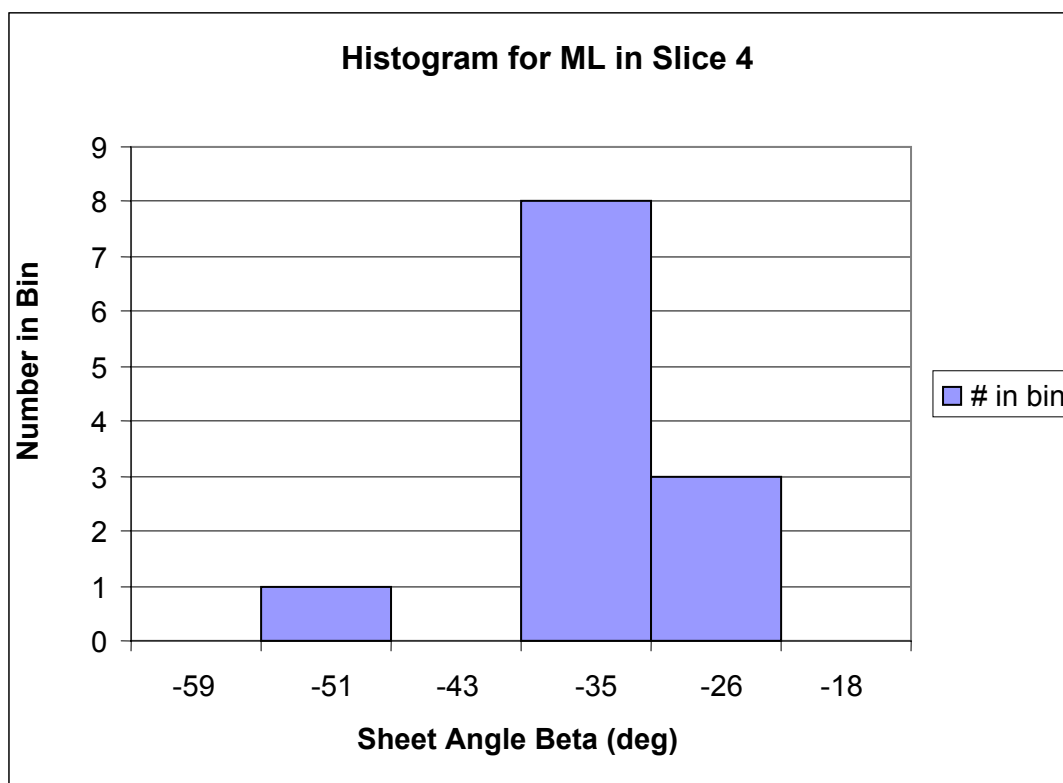


Fig. 4.7 Plot of sheet angles taken from slice four.



#### 4.5 *Three-Dimensional Reconstruction*

Once the fiber angle  $\alpha$  and sheet angle  $\beta$  were determined for each slice, we were then able to reconstruct a three-dimensional model based on these findings using a custom code that Dr. Criscione developed (fig. 4.8). The fiber and sheet angle at the center of each slice were put into the code to view the myolaminate morphology. From the two-dimensional images, hence, a three-dimensional model was created. The fiber angle varies linearly through the wall, yet the sheet angle is constant in each slice. While the model assumes that there is only one family of myolaminae, such models are currently state of the art. Future work will be directed towards describing better the myolaminate morphology that is directly observed.

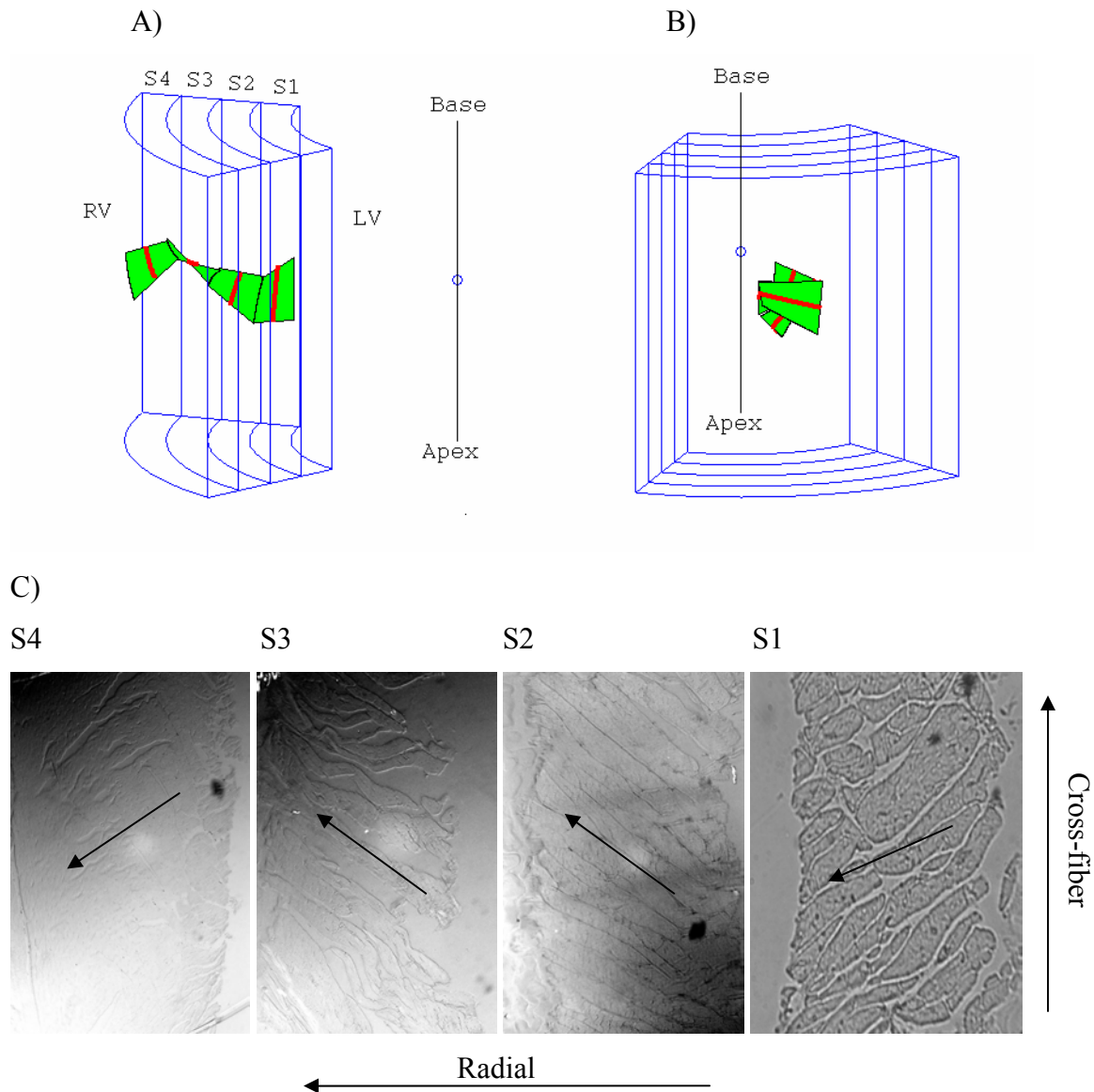


Fig. 4.8 Three-dimensional reconstruction using alpha and beta findings. A) Three-dimensional reconstruction as viewed from the anterior face of the heart. B) Three-dimensional reconstruction as viewed from the right side of the heart. C) Sheet images with estimated beta marked. (S1 looks different than the other three because it was imaged with a polarizer, the other three are bright field images.)

## CHAPTER V

### DISCUSSION

#### *5.1 Introduction*

This chapter will discuss the effectiveness of the new method that was created to improve the current quantitative analysis of the myocardium. The results from our testing of the method will also be addressed in this section. The purpose of this research was to improve the existing procedures of obtaining quantitative data from myocardial tissue by making it less time consuming and more cost effective. The new method that was devised will be discussed in terms of its rationale, experimental effectiveness, and relevance to the overall scheme of quantitative myocardial analysis.

#### *5.2 Discussion of Heart Removal and Preservation*

The removal and preservation of the heart went quite smoothly. We did, however, in our first trial, forget to take the weight of the heart upon removal which is something we will have to make sure we do in the future in order to compare the hearts. The method we used to fix the heart in diastole worked well and was quite easy. In the future we may need to consider how the central venous pressure changes as hearts begin to go into failure. We will have to decide if we want to use a constant venous pressure or possibly measure the venous pressure of the rat prior to sacrifice.

The fixation process was carried out in a timely manner. The tissue spent one week in the formalin fixative then was sliced and spent another week in the JB-4 embedding solution, then was cut again and placed in the JB-4 hardener for about three days after which it was sliced and imaged. The whole removal and preservation process from start to finish was completed in about 18 days. While 18 days may seem like a long time the nice part is that several hearts can be excised and fixed at the same time and a minimal amount of actual hands on time is required from the researcher.

### 5.3 *Discussion of Slicing and Orientation Techniques*

The slicing and orientation techniques seemed to work quite well in this method. The first cuts were made and imaged in about an hour, and the second round of cross-fiber cuts were made and imaged in about 2 hours. As can be seen little time is required by the researchers to actually cut the tissue for fiber and sheet angle viewing.

### 5.4 *Fiber Alignment*

The images of the fiber angles were fairly clear and easy to measure. As can be seen from Table 4.2 we took quite a few measurements to verify our findings and make sure that we obtained as accurate a fiber direction as possible for each slice. As mentioned before, based on the plot of the measurements and on the standard deviations, we were able to determine that the most efficient number of measurements was ten. Therefore, in the future when comparing multiple hearts, we will only take ten fiber measurements from each sheet.

### 5.5 *Sheet Alignment*

The images of the sheet angles looked great as can be seen in figure 4.2. We had no problems determining orientation with the positive cross-fiber marked and knowing, based on the slice, which side of the tissue the paper was placed. We did notice, once we started imaging the slices, that there were several sheet families within some of the slices. Because of this, we decided to change our method from averaging all the sheets in the region of interest, like was done for the fiber angles, to grouping the measured angles in bins after removing the largest and smallest angle. We then found the bin with the greatest number of measurements and took the average of that group. This allowed us to make sure we were actually measuring the dominate sheet angle within that particular slice. In the future, it may be beneficial to find the  $\beta$  of the other sheet families as well and incorporate them into our three-dimensional model. But for now, we feel that finding the dominate family will keep this method time efficient and suffice for comparing diseased and healthy hearts in the future.

Another issue that arose was the question of whether or not we were missing anything by not making more cuts. Since the sheets have a considerable radial

component, we feel that going any smaller with our slices would not have allowed us to take the sheet angle measurements as well. Many of the sheets would have been cut off and would have prevented us from knowing the true  $\beta$  direction.

We also noticed that as we imaged from the inner wall to the outer wall, the number of sheets seen became fewer. This may be due to the greater amount of displacement required by the inner wall. As a result, the inner wall requires more sheets to allow this movement compared to the outer wall in which there is less displacement.

### *5.6 Three-Dimensional Reconstruction*

Through our research we were able, by imaging several faces of the septum, to develop a method for obtaining a three-dimensional model from two-dimensional images in a timely and cost effective manner. While this method may not produce an exact replica of the septum, it does provide a good model for comparison. The final three-dimensional model is most accurate at the center of each slice due to the averaging that was done in order to reconstruct it. However, since we were able to take four slices fairly easily, this gives us a good idea of how the fiber and sheet angles are changing throughout the septum and will be an excellent model for seeing how the angles vary in both healthy and diseased rat hearts.

This will also allow for a better understanding of how stresses and strains develop within the heart wall and will allow for multiple comparisons to be done in both a timely and effective manner. We will be able to evaluate the hypothesis that the alignment of sheets in healthy hearts display reduced shear stress due to the shearing effects of the layers. Later, we will also be able to see how this changes in diseased hearts as the number of sheets begin to decrease, thus, allowing less slippage and greater stress development. As the stress increases the thickness to radius ratio will begin to decrease and eventually lead to heart failure.

### *5.7 Animal Model*

Dahl salt sensitive rats will be used as an animal model in future experiments since heart failure can be induced without surgical procedures (Dahl et al., 1968, Emery and Omens, 1997, Inoko et al., 1994, Nishina et al., 2002). Volume-overloaded cardiac

hypertrophy will be induced using high salt diets in Dahl salt sensitive rats. Over a 15-18 week time span, 10 of the rats will be fed an 8% NaCl (high salt) diet, while 10 will be fed a normal diet. An example of the composition (g/100g diet) consists of 7.0 water, 24.0 protein, 5.1 fat 6.2 ash, 3.2 crude fiber, 0.26 sodium, and 0.75 potassium (Inoko et al., 1994). The animal's general condition will be monitored every 24 hours. If they are found dead, they will be subject to immediate post mortem pathological examination. We expect to find the Dahl salt sensitive rats fed the high-salt diet developing rapid and labored respiration during the 15-20 week. Therefore, those that do not seem to be doing as well will be sacrificed at this stage so as to perfuse the heart and obtain the best model of cardiac hypertrophy. Fiber angle, sheet angle, myolaminate morphology, heart weight, septum thickness, and diameter will be assessed. Our hypothesis is that the myolamina of the inner wall will appear more like that of the outer wall because the shear strains in the inner wall, after chronic dilation, are more like that of the outer wall in the rats that went out the 17-20 week period. To test this hypothesis, for laminar thickness, for example, we will do an unpaired t test (difference of septum thickness in normals versus such a difference in Dahl rats). We will also sacrifice some of the Dahl rats at 16 weeks to evaluate the indications of the development of LV concentric hypertrophy. Our hypothesis is that the laminar thickness will be increased and the end diastolic radius will be decreased due to the overload of the heart. However, as the hearts continue in the overloaded state they will become quite large and the walls will begin to thin as seen in Inoko (1994)'s research (Fig. 5.1).

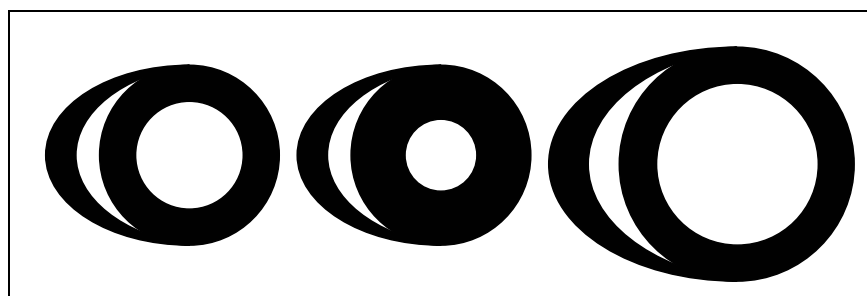


Fig. 5.1 Depictions of transverse tissue slices of the LV from Dahl salt-sensitive rats fed high salt diets at 6 wks, 11 wks, and 18wks respectively (after Inoko, 1994)

## CHAPTER VI

### CONCLUSIONS AND RECOMMENDATIONS

#### *6.1 Conclusions*

In this research, methods were developed to simplify the quantitative analysis of the interventricular septum of rat hearts. We were able to maintain orientation while obtaining images, and measuring the regions of interest. By doing this, we were able to reconstruct a three-dimensional model from the obtained results. This verifies our method and will allow future analysis to be done with the same method. Since this method was designed to be time and cost effective, it will be much easier to quantify larger numbers of hearts and therefore, compare both healthy as well as different types of diseased hearts at various stages of failure.

#### *6.2 Recommendations*

It would be a good idea to try this method on a few more healthy rats to confirm its consistency. Once this was verified, we could then continue with the diseased hearts and make the desired comparisons. Another possible recommendation would be to look at and measure all the sheet families in each slice. It would be interesting to see how this would change the three-dimensional model. The only negative side to doing this, however, would be that it would make the process more time consuming.

Over all, we feel that this is a good method for developing comparable three-dimensional models of the myocardium in rats. We believe that it will work well in future research on both healthy and diseased hearts. We also understand that quantifying diseased rat hearts is only the first step in a series of experiments that are needed to determine whether or not the laminar structure of the myocardium is capable of further differentiation at the adult stages or if it becomes static upon maturation. We know that pressure overloaded hypertrophy and that of volume overload are two extremes of the thickness to radius ratio with normal somewhere between these two. Therefore, we hope that studies with both pressure and volume overloaded adult rats and neonates will be

performed to better understand how the laminar structure of myocardium is formed and modulated as the heart grows and remodels.



## REFERENCES

- Arts, T., Costa, K.D., Covell, J.W., McCulloch, A.D., 2001. Relating myocardial laminar architecture to shear strain and muscle fiber orientation. *American Journal of Physiology* 280, H2222-H2229.
- Ashikaga, H., Criscione, J.C., Omens, J.H., Covell, J.W., Ingels, N.B., 2004. Transmural left ventricular mechanics underlying torsional recoil during relaxation. *American Journal of Physiology* 286, H640-H647.
- Braunwald, E. 2001. Heart failure. In: Hauser, S.L., Fauci, A.S., Longo, D.L., Jameson, J.L., Kasper, D.L. (Eds.), *Harrison's Principles of Internal Medicine*. McGraw-Hill, New York, p. 1318-1329.
- Berne, R.M., Levy, M.N., 2001. *Cardiovascular Physiology*. Mosby, St. Louis, pp.55-81.
- Caulfield, J.B., Borg, T.K., 1979. The collagen network of the heart. *Laboratory Investigation* 40, 364-372.
- Costa, K.D., Holmes, J.W., McCulloch, A.D., 2001. Modeling cardiac mechanical properties in three dimensions. *Philosophical Transactions Royal Society London* 359, 1233-1250.
- Costa, K.D., Takayama, Y., McCulloch, A.D., Covell, J.W. 1999. Laminar fiber architecture and three-dimensional systolic mechanics in canine ventricular myocardium. *American Journal of Physiology* 276, H595-H607.
- Dahl, L.K., Knudsen, K.D., Heine, M.A., Leitl, G.J. 1968. Effects of chronic excess salt ingestion. *Circulation Research* 22, 11-18.
- Deschepper, C.F., Picard, S., Thaibault, G., Touyz, R., Rouleau, J.L., 2002. Characterization of myocardium, isolated cardiomyocytes, and blood pressure in WKHA and WKY rats. *American Journal of Physiology* 282, H149-H155.
- Emery, J.L., Omens, J.H. 1997. Mechanical regulation of myocardial growth during volume-overloaded hypertrophy in the rat. *The American Physiological Society*, H1198-1204.
- Feldman, A.M., Weinberg, E.O., Ray, P.E., Lorell, B.H., 1993. Selective changes in cardiac gene expression during compensated hypertrophy and the transition to cardiac decompensation in rats with chronic aortic banding. *Circulation Research* 73, 184-192.

- Figueredo, V.M. Camacho, S.A., 1994. Basic mechanisms of myocardial dysfunction: cellular pathophysiology of heart failure. *Current Opinion in Cardiology* 9, 272-279.
- Gerdes, A.M., Capasso, J.M., 1995. Structural remodeling and mechanical dysfunction of cardiac myocytes in heart failure. *Journal of Molecular Cardiology* 27, 849-856.
- Grossman, William, 1980. Cardiac Hypertrophy: useful adaptation or pathologic process. *The American Journal of Medicine* 69, 576-583.
- Humphrey, J.D., 2002. *Cardiovascular Solid Mechanics*. Springer, New York, pp. 601-617.
- Inoko M, Kihara Y, Morii I, Fujiwara H, Sasayama S., 1994. Transiting from compensatory hypertrophy to dilated, failing left ventricles in Dahl salt-sensitive rats. *American Journal of Physiology* 267, H2471 – H2482.
- Komuro, I., Yazaki, Y., 1993. Control of cardiac gene expression by mechanical stress. *Annual Review of Physiology* 55, 55-57.
- LeGrice, I.J., Hunter, P.J., Smaill, B.H., 1997. Laminar structure of the heart: a mathematical model. *American Physiological Society*, H2466-H2476.
- LeGrice, I.J., Smaill, B.H., Chai, S., Edgar, S.G., Gavin, J.B., Hunter, P.J., 1995a. Laminar structure of the heart: ventricular myocyte arrangement and connective tissue architecture in the dog. *American Physiological Society* 269, H571-H582.
- LeGrice, I.J., Takayama, Y., Covell, J.W., 1995b. Transverse shear along myocardial cleavage planes provides a mechanism for normal systolic wall thickening. *Circulation Research* 77(1), 182-193.
- Matsumoto, T., Hayashi, K., 1996. Stress and strain distribution in hypertensive and normotensive rat aorta considering residual strain. *Journal of Biomechanical Engineering* 118, 62-73.
- Nielsen, P.M.F., LeGrice, I.J., Smaill, B.H., Hunter P.J., 1991. Mathematical model of geometry and fibrous structure of the heart. *American Physiological Society* 260, H1365-H1378.
- Nishina, T., Miwa, S., Yuasa, S., Nishimura, K., Komeda, M. 2002. A rat model of ischaemic or dilated cardiomyopathy for investigation left ventricular repair surgery. *Clinical and Experimental Pharmacology and Physiology* 29, 728-730.
- Omens, J.H., 1998. Stress and strain as regulators of myocardial growth. *Progress in Biophysics and Molecular Biology* 69, 559-572.

- Robinson, T.F., Cohen-Gould, L., Factor, S.M., 1983. Skeletal framework of mammalian heart muscle. *Laboratory Investigation* 49, 482-498.
- Robinson, T.F., Geraci, M.A., Sonnenblick, E.H., Factor, S.M., 1988. Coiled perimysial fibers of papillary muscle in rat heart: morphology, distribution, and changes in configuration. *Circulation Research* 63, 577-592.
- Sabbah, H.N., Sharov, V.G., 1998. Apoptosis in heart failure. *Progress in cardiovascular diseases* 40, 549-562.
- Sadoshima, J., Izumo, S., 1997. The cellular and molecular response of cardiac myocytes to mechanical stress. *Annual Review of Physiology* 59, 551-571.
- Schoen, F.J. 1999. The heart. In: Kumar, V., Collins, T., Robbins, S.L. Contran, R.S.(Eds.), *Robbins Pathologic Basis of Disease*. W.B. Saunders Company, Philadelphia, pp. 546-550.
- Streeter, D.D. Jr. 1979. Gross morphology and fiber geometry of the heart. In: *Handbook of Physiology: The Cardiovascular System. The Heart*. American Physiological Society, Bethesda, MD, sect. 2, vol. I, chapt. 4, pp. 61-112.
- Streeter, D.D. Jr., Bassett, D.L. 1966. An engineering analysis of myocardial fiber orientation in pig's left ventricle in systole. *The Anatomical Record* 155, 503-511.
- Young, A. A., LeGrice, I.J., Young, M.A., Smaill, B.H. 1998. Extended confocal microscopy of myocardial laminae and collagen network. *Journal of Microscopy* 192.2, 139-150.

## VITA

Emily Hope Jetton was born in Houston, Texas on November 1, 1979 to Bob and Peggy Jetton. Emily grew up in Conroe and attended Oak Ridge High School, from which she graduated in May of 1998. Emily studied biomedical engineering at Texas A&M University as an undergraduate student and received her B.S. in December of 2002. In the spring of 2003, Emily began her graduate work under Dr. John C. Criscione in biomedical engineering at Texas A&M University. In August of 2004, Emily received her M.S. in biomedical engineering. She began working for St. Jude Medical in June of 2004 and hopes to continue her career with this reputable company and continue gaining valuable work experience. Her permanent address is as follows:

Emily Hope Jetton  
300 East South Street #2003  
Orlando, FL